Green Chemistry

PAPER

View Article Online
View Journal | View Issue

Cite this: *Green Chem.*, 2026, **28**, 2736

Membranes from bio-based poly(ethylene furanoate) and natural solvents

Malinalli Ramírez-Martínez,[a] Usman T. Syed,[a] Glenda Terán-Cuadrado,[b,c] Anissa Nurdiawati,[a,c] Maria Di Vincenzo,[a] Iuliana M. Andrei,[a] Dimitrios N. Bikiaris,[d] Sami G. Al-Ghamdi[a,c] and Suzana P. Nunes *[a,b,e]

Replacing fossil materials with renewable bio-based alternatives is a pivotal strategy to make the membrane manufacturing industry more sustainable in alignment with the UN Sustainable Development Goals. Poly (ethylene furanoate) (PEF) is a biopolymer synthesized from 2,5-furan dicarboxylic acid, a natural monomer that can be derived from lignocellulosic biomass, with the potential to replace fossil polymers across various fields. However, its high chemical stability makes solubilization challenging, and currently, the most common solvent choices for this purpose are fossil-based solvents such as trifluoroacetic acid and hexafluoro-2-propanol. In this work, we introduce a bio-based solvent alternative to process PEF into porous membranes consisting of a deep eutectic system comprising the natural solids thymol and vanillin. The resulting ultrafiltration membranes exhibited competitive performance in fruit juice clarification. A life cycle assessment showed a lower global warming potential, human toxicity, and fossil depletion for the proposed fabrication protocol compared to a fossil-based counterpart, poly(ethylene terephthalate) solubilized in trifluoroacetic acid. We identified non-solvent production and waste treatment as the primary contributors to the environmental impact of PEF membrane production, and demonstrated the environmental benefits of mitigation strategies such as waste recycling, energy recovery, and the use of a bio-based non-solvent. Our findings expand the alternatives for more sustainable PEF processing in solution and demonstrate the potential of PEF as a high-performance polymer for membrane separation applications.

Received 12th October 2025,
Accepted 18th December 2025

DOI: 10.1039/d5gc05422b

rsc.li/greenchem

Green foundation

1. This work proposes a renewable system for polymeric membrane fabrication by phase inversion utilizing the bio-based polymer poly(ethylene furanoate) (PEF) with thymol and vanillin as green solvent components.
2. This system poses reduced hazards compared to fossil-based solvents for PEF solubilisation. The PEF membrane preparation approach has a 42% lower global warming potential compared to fossil-based PET membranes of comparable filtration ranges. Further life cycle assessment modelling optimization indicated significant reduction of the impact by employing bioethanol and waste recycling.
3. The environmental performance of this work could be improved with greener synthesis of the polymer and natural solvents, usage of high molecular weight bio-based polymers for improved properties, and solvent recycling strategies. Identifying other water-miscible green solvents for PEF could further reduce the environmental impact, preventing the use of ethanol in the coagulation bath.

[a]*Environmental Science and Engineering Program, Biological and Environmental Science and Engineering Division (BESE), King Abdullah University of Science and Technology (KAUST), 23955-6900 Thuwal, Saudi Arabia.*
E-mail: suzana.nunes@kaust.edu.sa
[b]*Chemical Engineering Program, Physical Sciences and Engineering, King Abdullah University of Science and Technology (KAUST), Thuwal, 23955-6900, Saudi Arabia*
[c]*KAUST Climate and Livability Initiative, King Abdullah University of Science and Technology (KAUST), Thuwal, 23955-6900, Saudi Arabia*
[d]*Laboratory of Polymer Chemistry and Technology, Department of Chemistry, Aristotle University of Thessaloniki, GR-54124 Thessaloniki, Greece*
[e]*Chemistry Program and Chemical Engineering Program, Physical Science and Engineering Division (PSE), King Abdullah University of Science and Technology, Saudi Arabia*

1. Introduction

Plastic pollution has a persistent negative impact on the environment, with contributions from the synthesis to the end of the life cycle.[1,2] Its production mainly uses fossil chemicals as starting materials and fossil energy for synthesis and processing. Currently, 6% of the oil production worldwide, higher than 400 million tons per year, is used for polymer manufacture.[3,4] In a broader perspective, the complex and interconnected environmental challenges we face demand changes in the materials production pathways across all sectors.[5] In the polymer field, this has motivated a race toward

renewable materials, sustainable alternative feedstocks, and synthesis processes that move away from oil refinery technologies.[6]

The use of biomass as feedstock, directly extracting the needed monomers or modifying others and polymerizing, is an attractive strategy, especially considering non-edible lignocellulosic biomass sources.[4,7,8] For instance, renewable plant oils and sugars are being used to produce monomers for polyacetals, polyoxalates, polyamides, *etc*. Sugar-based monomers are hydrophilic and plant oil-based monomers are hydrophobic.[9–11] Long-chain aliphatic polyesters can be synthesized from fatty-acid monomers such as sebacic acid, ω-hydroxydecanoic acid and ε-decalactone obtained from plant oils; polycarbonates or polyurethanes from monomers like pinanediol and polyols derived from cyclic terpenes or vegetable oil; poly(hydroxyl alkanoates) (PHAs) *via* microbial fermentation; and polyacetals from monomers derived from carbohydrates, terpenoids, and lignin such as xylitol, citronellal and propylguaiacol.[7,10] Some of these polymers can present improved thermal stability, mechanical strength, or biodegradability.

Currently, only about 0.6% of the globally produced polymers are bio-derived,[4,12] which can be related to the long steps of process optimization and industrial certification that any new product reaching the market requires. There are challenges, but also many opportunities in the establishment of biorefineries for bio-based polymer production with a competitive cost, which is high compared to those of fossil-based polymers.[13,14] Currently, the largest application of bio-based polymers is in packaging and fibers. Poly(lactic acid) shares 42% of the globally produced capacity, followed by poly(hydroxy alkanoates) (PHAs) with a value of 17%.[12]

Polymer membrane technology for separation processes is a key enabler for the sustainable production of a wide variety of products due to its lower energy consumption, scalability, and ease of operation compared to traditional thermal separation methods.[15] Membranes have already improved the energy footprint in various fields, including wastewater treatment, potable water production, food processing, and the medical sector. Extending the impact of membrane technology to the chemical industry and other applications requires membranes that resist harsh, long-term operation. High-performance polymers stable in various solvents would be the most adequate for membrane fabrication for processes under demanding conditions. We previously investigated polytriazole and poly(ethylene terephthalate) (PET), among others, for this purpose.[16,17] However, despite the operational advantages of membranes in separation processes, sustainability must be analyzed from a holistic perspective.

Polymer membranes are mainly manufactured by the phase separation of dope solutions induced by contact with a non-solvent or by a temperature change.[18–21] In current industrial membrane manufacturing, fossil-based polymers and solvents are common choices, given their wide availability, affordability, and high technology readiness level.[22] Polymers frequently used for membrane fabrication include polysulfone (PSf), polyethersulfone (PES), poly(vinylidene fluoride), and polyethylene. Typical solvents are *N*,*N*-dimethylformamide (DMF), *N*,*N*-dimethylacetamide (DMAc), *N*-methyl-2-pyrrolidone (NMP), and tetrahydrofuran. Health concerns are growing regarding the broad use of these solvents due to their toxicity and persistence in the environment. This resulted in the development of policies to reduce the use of these chemicals on an industrial scale. For instance, the European Chemicals Agency has already restricted the occupational exposure to DMF, NMP, and DMAc in the European Union.[23] Therefore, the gradual replacement of fossil-based materials in the membrane industry with more sustainable alternatives, such as bio-based polymers and solvents, is compulsory.[15,24–26]

The integration of biopolymers and bio-based solvents for sustainable membrane fabrication is a topic of growing academic interest and industrial demand. Recent reports include systems such as PHAs in cyrene,[27] lignin in a 2 : 1 propionic acid : urea mixture,[28] polylactic acid in methyl lactate,[29] and cellulose in triethyl phosphate.[30] Other synthetic and natural bio-based polymers are being explored for applications other than membrane fabrication. Examples are humins, sporopollenin, and cutin.[31] Therefore, additional studies of bio-based polymer membranes fabricated with bio-based solvents are needed to further diversify the sustainable choices for industrial membrane manufacturing and enable the most challenging dissolution of polymers and starting materials.

Biopolymers derived from furanic monomers, such as 2,5-furan dicarboxylic acid (FDCA), constitute an emerging class that can be synthesized from lignocellulosic biomass. FDCA holds potential as a building block for the bioeconomy and is listed among the top twelve value-added chemicals from biomass according to the U.S. Department of Energy.[32] Poly (ethylene furanoate) (PEF) is the most developed FDCA-based polymer, starting to be commercially available. The properties of PEF resemble those of PET (which currently accounts for 6.2% of plastics produced worldwide[33,34]), and it is considered for its potential replacement.[35,36] Compared to PET, PEF has superior gas barrier properties,[37,38] being particularly attractive for food, beverages, and cosmetics packaging.[39,40] For the membrane industry, PEF could address two main challenges: fabrication sustainability and stability under demanding conditions.

Currently, only a small number of studies have examined the development of FDCA or PEF-based membranes, given the challenging solubility of this polymer class. These studies rely on fossil-based solvents like hexafluoro-2-propanol or trifluoroacetic acid as the main solvent in combination with dichloromethane and/or dichloroethane as the cosolvent, mostly employing the electrospinning technique.[41–45] However, solution casting and immersion in a non-solvent are the preferred method of membrane fabrication. The critical challenge remains in substituting fossil-based and toxic solvents with more sustainable alternatives, which could have environmental benefits for the membrane manufacturing industry

and other processes requiring solubilization of PEF, such as dissolution-based recycling.[46]

As crucial as exploring feasible routes for membrane preparation from bio-derived polymers and natural solvents is having a holistic evaluation of the environmental impact of the whole process, leading to the final product.[47,48] Life Cycle Assessment (LCA), as defined by ISO 14040/14044, is a valuable methodology to identify, classify, and quantify the material and energy inputs/outputs in a production system and their associated environmental impact.[49] In membrane technology, LCA has been more frequently considered for applications such as water treatment, food processing, hydrogen production, and carbon capture.[50–53] It has been less applied to the membrane fabrication itself. Evaluation of sustainable membrane fabrication has indicated a lower environmental impact associated with the use of biopolymers and green solvents.[54–57]

Herein, we report for the first time the use of a natural solvent mixture consisting of thymol and vanillin for the solubilization of PEF and subsequent membrane fabrication. We investigated the solvent and solvent–polymer interactions, determined the effects of the polymer concentration and temperature of the coagulation bath on the membrane properties, and explored the application of the resulting membranes for clarification of fruit juice. Moreover, we assessed the environmental impact of our fabrication approach *via* LCA. We elucidated the hotspots within our approach for PEF membrane manufacturing with natural solvents and compared its environmental performance to that of its fossil-based counterpart, PET solutions in TFA. Overall, we demonstrate the potential of thymol and vanillin mixtures for PEF solubilization and membrane manufacturing to advance the sustainability of membrane technology and biopolymer processing.

2. Experimental section

Materials and chemicals

2,5-Furan dicarboxylic acid (bio-FDCA X000230-2003) was purchased from Corbion (Gorinchem, the Netherlands). Vanillin (99%) was purchased from Thermo Scientific. Trifluoroacetic acid (99%) was purchased from Alfa Aesar. Ethanol absolute was obtained from VWR chemicals. Thymol (>98.5%), ethylene glycol (anhydrous, 99.8%), antimony trioxide, and polyethylene glycol (PEG) standards of different molecular weights were purchased from Sigma-Aldrich. All chemicals were used without further purification. Milli-Q water was used for water filtration tests. Natural fresh apple, orange, and pomegranate juices for clarification tests were obtained from a local store.

Solvent screening

The solvent selection was initially based on the Hansen Solubility Parameters (HSPs) of 20 green solvents reported for membrane manufacturing or polymer solubilization. In the HSP approach, the affinity between solvent 1 and polymer 2 can be estimated by their Relative Energy Difference (RED), given using eqn (1) and (2):

$$\mathrm{RED} = R_a/R_0 \quad (1)$$

$$R_a{}^2 = 4(\delta_{d2} - \delta_{d1})^2 + (\delta_{p2} - \delta_{p1})^2 + (\delta_{hb2} - \delta_{hb1})^2 \quad (2)$$

where R_a is the distance between the solvent and polymer in the Hansen space; R_0 is the interaction radius of the polymer; and δ_h, δ_p, and δ_d, are the hydrogen, polar, and dispersion parameters. If the RED has a value smaller than 1, there is a high likelihood of polymer dissolution. HSPiP software, version 6.0.04, was used to calculate the theoretical HSP values for PEF based on its Simplified Molecular Input Line Entry System (SMILES) obtained *via* ChemDraw software (PEF SMILES: XO═C(OCC)C1═CC═C(C([O])═O)O1X). The interaction radius was 8.0 $MPa^{0.5}$. The solvents were sorted based on the RED between the solvent and PEF.

PEF membrane fabrication

PEF membranes were prepared by Non-solvent Induced Phase Separation (NIPS). A mixture of thymol and vanillin in a molar ratio of 4 : 1 was prepared by heating them at 90 °C under stirring until fully dissolved. The resulting mixture was cooled down to room temperature and used within 2 days. The dope solution was then prepared by the addition of 18 wt% PEF content in the solvent mixture. The solution was stirred at 150 °C in a silicon oil bath, and once the polymer was fully dissolved, the temperature was decreased to 120 °C. The obtained solution was cast with a casting rod with a 250 μm gap on a glass plate at 75 °C. The film was then immersed in a coagulation bath containing ethanol at 20 or 4 °C for membrane formation. The ethanol amount was 100 ml per gram of dope solution. The membrane was washed with ethanol for 24 hours and allowed to dry at room temperature for 24 hours.

Materials characterization

Intrinsic viscosity measurements for the PEF polymer were performed using an Ubbelohde viscometer (Schott Gerate GmbH, Hofheim, Germany) at 30 °C in a mixture of phenol/1,1,2,2-tetrachloroethane at a ratio of 60/40 w/w. A sample concentration of 1% (w/v) was used. The synthesized PEF had an intrinsic viscosity of 48 ml g^{-1}, determined with the Ubbelohde viscometer with a protocol previously reported,[58] which according to the Berkowitz Equation corresponds to an average number molecular weight (M_n) of 10 600 g mol^{-1}. Proton (^1H) and carbon (^{13}C) Nuclear Magnetic Resonance (NMR) spectra were recorded using a Bruker Avance III operating at 600 MHz. The solvent was $CDCl_3$ for thymol and vanillin samples, and deuterated trifluoroacetic acid for PEF samples and solutions. UV-Vis spectra of thymol–vanillin solutions were recorded using a PerkinElmer Lambda 950 spectrometer with a quartz cuvette at room temperature. Fourier transform infrared (FTIR) analysis was performed using a Nicolet iS10 instrument (Thermo Fisher Scientific) from 500 to 3800 cm^{-1} with 32 scans.

Differential Scanning Calorimetry (DSC) analysis was performed using TA-DSC 250 equipment with Tzero hermetic pans. For pure polymer analysis, a heating–cooling–heating cycle with an upper temperature limit of 300 °C was performed with a cooling–heating rate of 10 °C min^{-1}. For PEF solutions, the upper temperature limit was 200 °C. In each upper or lower temperature limit, the sample was kept at a constant temperature for 5 minutes before the next heating/cooling step. Thermal degradation of the polymer was recorded using a thermogravimetric analyzer (TA-TGA 5500).

Optical microscopy was performed using a Leica DM 750P microscope. Two types of observations were made: (i) solution cooling under polarized light and (ii) solution phase separation *via* the infinite layer method. For (i), a Linkam LTS420 heating stage connected to an LNP96-S accessory was utilized for controlled cooling of the polymer solution at 50 °C min^{-1}. Observations were made under polarized light. For (ii), a drop of solution (approximately 2 μl) was placed on a standard microscope glass slide and covered with a 100 μm-thick glass. Double-sided tape was placed on two edges to create a 100 μm gap, and excess ethanol was added through one of the open sides to promote polymer precipitation. The polymer demixing rate (ν) was calculated as the ratio between the thickness of the precipitated polymer at a specific time (in this work, between 27 and 30 seconds).

Membrane characterization

The membranes were imaged using a Zeiss Merlin Electron Microscope field-emission scanning electron microscope (SEM) at 5 kV. Samples for cross-section observations were prepared by breaking a piece of membrane in liquid nitrogen and placing it between two layers of conductive carbon tape. Silver paint was used on the borders of the membrane pieces to improve contact between the carbon tape and the membrane. All samples were coated with a 6 nm iridium layer in a Quorum Q300RT sputter coater. Mechanical properties were obtained from strain *vs.* stress measurements using a Discovery DMA850 instrument, with a stress ramp set from 0.05 N to 18.00 N at a rate of 1.5 N min^{-1}. The reported values are the average of three measurements. The Grazing Incidence Wide-Angle X-ray Scattering (GIWAXS) diffractogram was obtained using a Xenocs Xeuss 3.0 instrument. Water contact angles were measured using an FM40 Easy Drop instrument (KRÜSS) with a drop volume of 2 μl. Surface pore size distribution analysis was performed using SEM images with an AI-based model developed by Thya Technology (https://www.linkedin.com/company/thya-technology).

The pore size distribution was measured by a second method, using a POROLUX 1000 gas–liquid displacement capillary flow porometer (Porotech). For that, the membrane pores are filled with Porefil, using a sample area of 2.99 cm^2. Nitrogen gradually pressurizes the membrane. The pressure at which the gas starts to freely flow is correlated with the largest pore by the Laplace equation and further increasing pressures gives the distribution of smaller pores.

Membrane performance

Initial performance evaluations were carried out in dead-end Amicon cells with membrane areas of at least 4.1 cm^2 attached to feed reservoirs and pressurized at 0.2 bar with nitrogen. For the determination of molecular weight cut-off (MWCO), the concentration of poly(ethylene glycol) with different molecular weights in the feed (C_f), retentate, and permeate (C_p) was determined by gel permeation chromatography (GPC) using an Agilent Technologies G1312B chromatography system with two PL aquagel–OH columns. Solute rejections (R) were calculated according to eqn (3):

$$R = \left(1 - \frac{c_p}{c_f}\right) \times 100\% \quad (3)$$

Juice clarification tests were performed on pomegranate, apple, and orange juices in dead-end and cross-flow configurations. In all cases, fresh juice was pretreated by centrifugation at 10 000 rpm for 10 min, followed by Whatman 113V filter paper. The pretreated juice was stored at 4 °C and used within 3 days. Before juice filtrations, all membranes were pre-compacted with pure water. During the filtration experiments, the weight of the permeate was recorded, and the flux was calculated according to eqn (4):

$$Q = \frac{V}{A \cdot t} \quad (4)$$

where V is the volume of the permeate, A is the area of the membrane, and t is the filtration time. The weight reduction factor (WRF) was calculated using eqn (5), while the permeate recovery (PR) was calculated using eqn (6), as follows:

$$\mathrm{WRF} = \frac{W_F}{W_R} \quad (5)$$

$$\mathrm{PR} = \frac{W_P}{W_F} \times 100\% \quad (6)$$

where W_F, W_R, and W_P are the weights of the feed, retentate, and permeate, respectively.

Dead-end experiments were carried out with Amicon stirred cells with a membrane effective area of at least 4.1 cm^2 pressurized with nitrogen gas to 0.2 bar. In cross-flow experiments, the volumetric feed flow rate was set at 950 mL min^{-1}. The membrane effective area was 20.6 cm^2. A polyester non-woven support was placed behind the PEF membrane to minimize damage. Hydrodynamic analysis using a hydraulic diameter of 1.6 mm and the properties of unclarified pomegranate juice at 20 °C (density ≈ 1073 kg m^{-3}; viscosity ≈ 3.49 mPa s) yielded a Reynolds number of ~360, confirming laminar flow.

In the dead-end configuration, membrane backwashing was simulated by flipping the membrane within the Amicon cell and running Milli-Q water through it for 30 min at 0.4 bar. Pomegranate juice clarification was also evaluated for commercial polyethersulfone (Synder MK-30 kDa) and polysulfone (Solecta M-PS20-GPP) membranes for comparison purposes.

Analytical methods for juice characterization included soluble solids, turbidity, color, and pH. Refractive index and

percent sucrose were recorded with an AR2008 refractometer (Krüss) and expressed as °Brix, as an indirect indication of the soluble solids. The turbidity was measured with a Micro 100 turbidity meter (HF Scientific). Color was measured as the absorbance at 420 nm using a Nanodrop 2000c instrument in the cuvette mode. The juice samples were measured with no dilution for apple and orange juices, while pomegranate juice was diluted to 20 v% with water. The pH was recorded with an AB150 pH meter (Accumet).

Life cycle assessment (LCA)

A comparative cradle-to-gate analysis in compliance with ISO 14040 and 14044 standards was conducted, including the industrial production of material and energy inputs, the membrane production at the laboratory scale, and waste generation from membrane fabrication. 1 m^2 of free-standing PEF or PET membrane was selected as FU, considering a weight/area ratio of 33.9 g m^{-2} based on experimental measurements. The life cycle impact assessment was performed using LCA for Experts software version 10.9.1.17 with its 2025.1 version database and ecoinvent 3.9.1 cut-off database, including environmental indicators from the ReCiPe 2016 v1.1 (H) midpoint method. More details are provided in the SI.

3. Results and discussion

The PEF used in this work was synthesized *via* a two-stage polycondensation method reported previously[59] (SI Fig. S1). The polymer average number molecular weight (M_n) was 10 600 g mol^{-1} as calculated from intrinsic viscosity measurements. The chemical and thermal characterization of the polymer is detailed in SI Fig. S2 and S3. The thermal analysis (SI Fig. S3) indicated a glass transition temperature of 83 °C, in the range of previously reported batches.[59] No degradation was detected up to 350 °C.

Solvent selection

Similar to PET, PEF exhibits high chemical stability and low solubility in most solvents typically used for membrane fabrication. Among the few reported solvents are trifluoroacetic acid, dichloromethane, dichloroethane, and hexafluoro-2-propanol.[42] To replace such harsh solvents with a more sustainable alternative, we performed a green solvent screening employing Hansen Solubility Parameters (HSPs) and Relative Energy Difference (RED) theory (SI, eqn (S1) and (S2)). Twenty green solvents were selected from the literature, where they have been reported for membrane fabrication or polymer solubilization as individual components or mixtures. From this initial screening, we selected vanillin and thymol, the only ones promising, given the RED <1 in relation to PEF (SI Fig. S4, SI Table S1). Both solvents are more sustainable than fossil-based solvents reported for PEF solubilization, as shown in Table 1. They are bio-based and readily biodegradable. They present no human toxicity, and their low vapour pressure can reduce exposure during handling. Their boiling points above 200 °C can allow for processability at more elevated temperatures. However, their prices are considerably higher than those of fossil-based solvents.

Thymol and vanillin are solids at room temperature, with melting points of 51.5 °C and 81.5 °C, respectively. Our previous work on thymol-based polyetherimide solutions revealed that strong hydrogen bond interactions can lead to the formation of homogeneous liquid solutions after polymer solubilization at high temperature, followed by cooling to room temperature.[60] PEF successfully solubilized in both thymol and vanillin, as single solvents, at 150 °C within 2 hours, forming homogeneous solutions with up to 20 wt% polymer, but they phase-separated upon cooling down to 110 °C. Besides the challenges of casting solutions above 110 °C, the resulting membranes had poor mechanical stability. Moreover, the viscosity of the dope solution was not ideal for film casting. Our next attempt was to employ a deep eutectic system comprising a mixture of thymol and vanillin. Deep eutectic systems typically have a melting temperature significantly lower than that of its pure components, with interactions driven mainly by hydrogen bonding, occasionally reinforced by van der Waals forces.[61] To the best of our knowledge, thymol–vanillin has never been used as a solvent for membrane fabrication. However, there are a few reports of this mixture for other applications, such as extraction of pesticides from olive oil[62] and PHAs from microbial biomass.[63,64] In one of these reports, Soltani *et al.*[62] confirmed the hydrogen bonding interactions by FTIR. They observed a shift in the O–H stretching vibrations of vanillin and thymol from 3254 cm^{-1} and 3228 cm^{-1}, respectively, to higher wavenumbers (3454 cm^{-1}). We con-

Table 1 Comparison of solvent properties between thymol, vanillin, and other solvents reported for PEF solubilization

Chemical	Source bio/fossil	Biodegradability	Human toxicity	Boiling point (°C)	Vapour pressure (mmHg at 25 °C)	Bulk price ($ per kg)
Thymol	Bio	High	No	233	1.60×10^{-2}	21 (natural)
Vanillin	Bio	High	No	285	1.18×10^{-4}	218 (natural) 49 (synthetic)
Trifluoroacetic acid	Fossil	Low	Moderate	72	1.10×10^{2}	8
Hexafluoro-2-propanol	Fossil	Low	Yes	58	1.59×10^{2}	2
Dichloromethane	Fossil	Moderate	Yes	40	4.38×10^{2}	0.45
1,2-Dichloroethane	Fossil	Low	Yes	84	7.70×10^{1}	3
Phenol	Fossil	Moderate	Yes	182	3.50×10^{-1}	0.85
1,1,2,2-Tetrachloroethane	Fossil	Low	Yes	146	5.74×10	11

ducted a systematic investigation by ^{1}H NMR analysis and confirmed the hydrogen bonding for a series of thymol–vanillin mixtures by a shift in the signal corresponding to the hydroxyl group of thymol from 4.86 (pure thymol) to 5.05, 5.26, and 5.72 ppm for thymol–vanillin molar ratios of 4 : 1, 1 : 1 and 1 : 4 (Fig. 1b), similar to what we previously observed for other systems containing thymol.[60]

In this work, PEF was fully solubilized in thymol–vanillin at a molar ratio of 4 : 1 at 150 °C, and the dope solution remained homogeneous when stored at 120 °C and cast at 75 °C. Notably, the initially clear colorless solution became purple after 30 minutes of heating at 150 °C (Fig. 1h). To better understand this phenomenon, we studied the color change of pure vanillin and thymol–vanillin solutions. Vanillin alone changed from yellow to orange after about 1 hour at 150 °C (Fig. 1c and f). On the other hand, 4 : 1 thymol–vanillin changed initially from yellow to brown and further to dark blue after about 4 hours (Fig. 1d and g). No evident chemical changes were detected by ^{1}H NMR and ^{13}C NMR for thymol/vanillin solutions after heating at 150 °C for 7 hours, despite the change in color (SI Fig. S5). These observations suggest that the color change in the vanillin-containing mixtures is caused by chemical interactions between the components, rather than simple thermal oxidation.

We hypothesize that also the interaction between PEF, thymol, and vanillin, allowing for PEF solubilization, is mainly driven by hydrogen bonding, while the color change might be related to vanillin keto–enol tautomerism (Fig. 1a, SI Fig. S6).

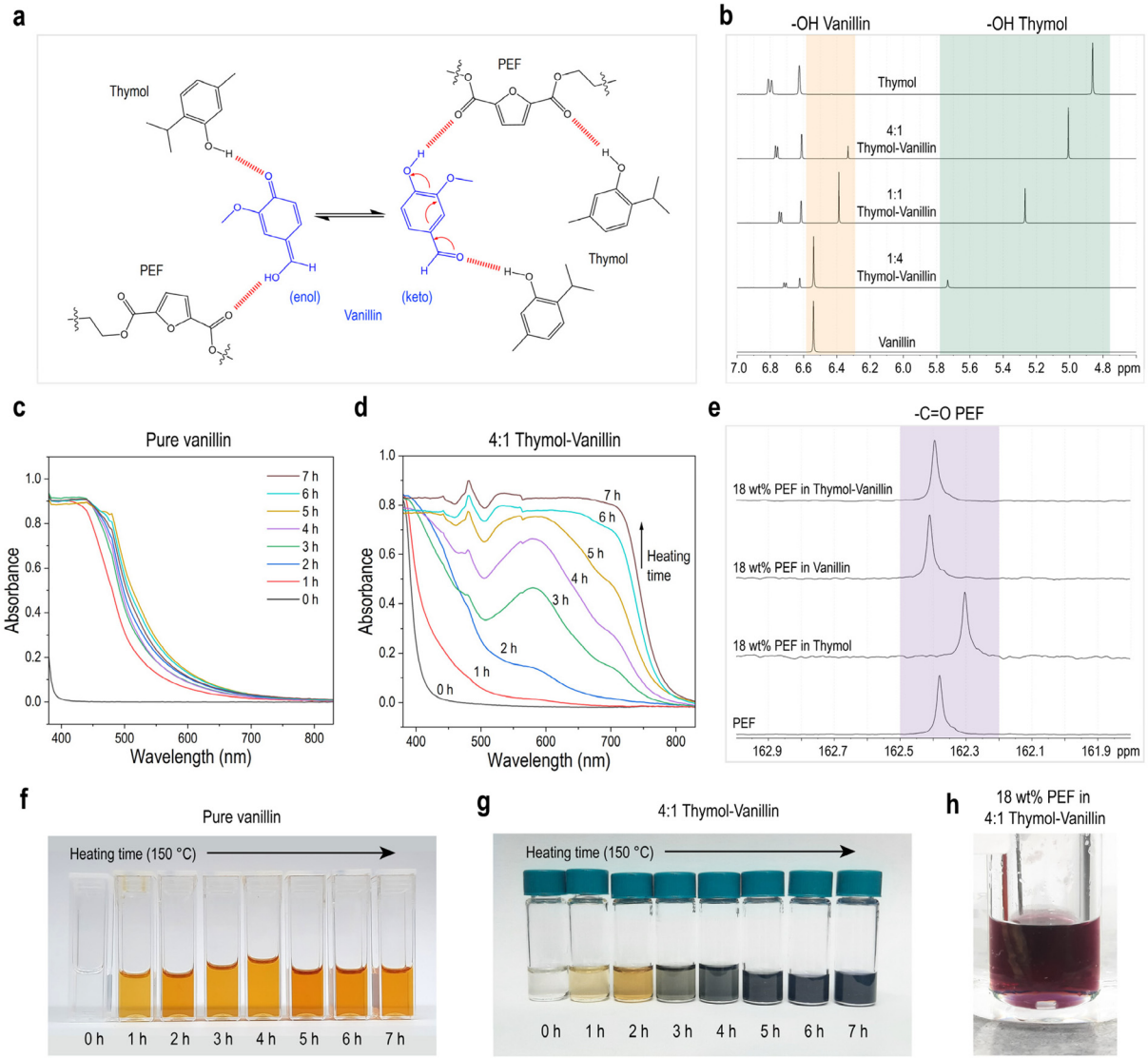

Fig. 1 Interactions between PEF, thymol, and vanillin. (a) Representation of the hydrogen bonding between PEF, vanillin (enol), vanillin (keto), and thymol. (b) ^{1}H NMR spectra of thymol–vanillin at different ratios. (c) UV-Vis spectra and (f) photographs of pure vanillin heated at 150 °C for different times. Samples were dissolved in ethanol with a 20 v% concentration. (d) UV-Vis spectra and (g) photographs of 4 : 1 thymol–vanillin heated at 150 °C for different times. (e) ^{13}C NMR spectra of pure PEF and 18 wt% PEF solutions in thymol, vanillin, and 4 : 1 thymol–vanillin. (h) Photograph of an 18 wt% PEF solution in 4 : 1 thymol–vanillin.

Photochromism linked to tautomerism has been observed in other phenol-containing systems like phenol-imidazole or Schiff base cyclic derivatives with nitrogen atoms.[65,66] The effect in those cases is a result of intramolecular proton transfer leading to a change of the π-electronic structure and stabilization of a tautomer by resonance. In the previously reported cases, vanillin-derived molecules in the keto form are in the most stable state, with the proton donor group –OH attached to the aromatic ring. The absorption spectrum depends on the extent of π-conjugations and possible electronic transitions linked for instance to double bonds (→ π*) and lone pairs of carbonyl groups (n → π*), both requiring relatively low energy. Tautomerism is affected by the molecular environment, particularly by the solvent and temperature. In the system investigated here, tautomerism is not induced by photochromism, *i.e.* light incidence, but rather is thermally driven. Strong hydrogen bonds between vanillin and thymol, and with PEF, stabilize one of the tautomer forms. Each tautomer exhibits a unique absorption spectrum due to differences in its electronic structure, resulting in distinct perceived colors. Longer wavelengths (*e.g.* brown and yellow) are associated with lower energy transitions. Tautomers with higher conjugation typically absorb at longer wavelengths (brown). The colors we see reflect the wavelengths that are not absorbed by the solution. Thus, when a more conjugated tautomer predominates, absorbing in yellow to brown (590–700 nm), it appears violet or blue, as observed in the PEF–vanillin–thymol system (Fig. 1d, SI Fig. S7). Vanillin tautomerism was further confirmed by spectroscopic analyses of pure vanillin with a strong protonating reagent, TFA, as detailed in SI Fig. S8 and S9. ^{1}H NMR and ^{13}C NMR spectra obtained for PEF mixtures with thymol and vanillin in TFA-d are shown in SI Fig. S10 and S11, respectively. A shift of the PEF carbonyl signal upfield when dissolved in pure thymol and downfield when dissolved in pure vanillin or thymol–vanillin is seen in the ^{13}C NMR spectra and highlighted in Fig. 1e. This is likely to be caused by carbon shielding–deshielding upon hydrogen bond formation,[67,68] which has been observed before for large derivatives of vanillin.[67] In the ^{1}H NMR spectra shown in SI Fig. S10, the OH signal for the mixtures containing thymol and vanillin is absent due to the strong hydrogen bonding with TFA-d, the solvent used for spectral acquisition. Therefore, we also recorded a series of ^{1}H NMR spectra in 1,1,2,2-tetrachloroethane-d2 as a deuterated solvent. The acquisition was performed from 25 to 140 °C (SI Fig. S12) to observe if and how the hydrogen bonding in the system is affected by temperature. By increasing the temperature, there is a decrease of the population of H-bonded sites over non-bonded ones. The strength of the H-bonds is typically between 2.4 and 9.5 kcal mol^{-1}.[69] For a simple estimation of the statistical population of bonded and non-bonded (free) hydrogen in the system, we could use the Boltzmann equation (eqn (7)):[70]

$$\frac{N_{\text{bonded}}}{N_{\text{free}}} = e^{-\Delta G/\text{RT}} \quad (7)$$

Bonding is exothermic and if we consider $\Delta G \approx -2.4$ kcal mol^{-1}, the values would be 58 at 25 °C, 33 at 75 °C and 22 at 120 °C. The polymer solution is cast at 75 °C, a condition at which the solvent–polymer hydrogen bond is enough to stabilize a homogeneous one phase system. The OH peaks in the ^{1}H NMR spectra reflect the population ratio of $N_{\text{bonded}}/N_{\text{free}}$ sites. As the equilibrium shifts toward the non-bonded state with an increase in temperature, the hydroxyl proton becomes more shielded. The chemical shift moves accordingly from 4.9 ppm at 25 °C to 4.4 ppm at 140 °C. Furthermore, the OH peak narrows as the temperature increases and is broader at lower temperatures. The peak of other protons, such as thymol CH_3 groups, remains practically unchanged. The sharp OH signals at high temperature are typical of a larger population of free fast exchanging protons. The spin–spin relaxation times ($T2$) also play a role. Weaker interactions between neighboring spins enable them to retain a coherent state for a longer period. $T2$ is then longer, and this contributes to a sharper peak.

Membrane formation and properties

While thymol and vanillin proved to be an excellent solvent choice for the dope solution, there is one additional challenge for membrane fabrication. They are both non-polar and their miscibility with water is restricted. For effective solvent–non-solvent exchange during membrane pore formation, the solvent and non-solvent should be miscible. We then considered choices of commercially available and non-toxic non-solvents to substitute water, and therefore, ethanol was selected. A set of six different conditions was tested for PEF membrane fabrication: 15, 18, or 21 wt% PEF solutions in thymol–vanillin, and ethanol as a non-solvent at 20 or 4 °C, following the protocol depicted in Fig. 2a.

To elucidate the phase separation mechanism and determine whether it was a thermally induced phase separation or driven by solvent exchange, we conducted two types of optical microscopy experiments: (1) heating–cooling of the dope solution under polarized light, and (2) live observation of phase separation, similar to previously reported procedures.[71,72] A liquid–solid phase separation of solutions of semicrystalline polymers can be observed as the nucleation and growth of spherulites, which constitute the birefringent phase, proceed. They can be distinguished under polarized light.[20,72] The liquid–solid phase separation with the formation of PEF spherulites was observed after one hour at room temperature (SI Fig. S13). While crystallization occurs, the process is too slow to have a significant influence on membrane formation,[59] which happens in a short time (<1 min), resulting in an amorphous system as confirmed by XRD (SI Fig. S14). DSC analysis of the 18 wt% PEF dope solutions in 4 : 1 thymol–vanillin was performed. At the investigated heating–cooling rates of 2.5 to 10 °C min^{-1}, we did not observe any transition that could indicate polymer crystallization (SI Fig. S15).

Optical microscopy imaging of a ~150 μm thick layer of polymer solution between cover glasses in contact with the non-solvent (ethanol) clearly shows pore formation by solvent–non-solvent exchange (Fig. 2c and e, SI Fig. S16–S18). Membrane pores are formed by liquid–liquid phase separation

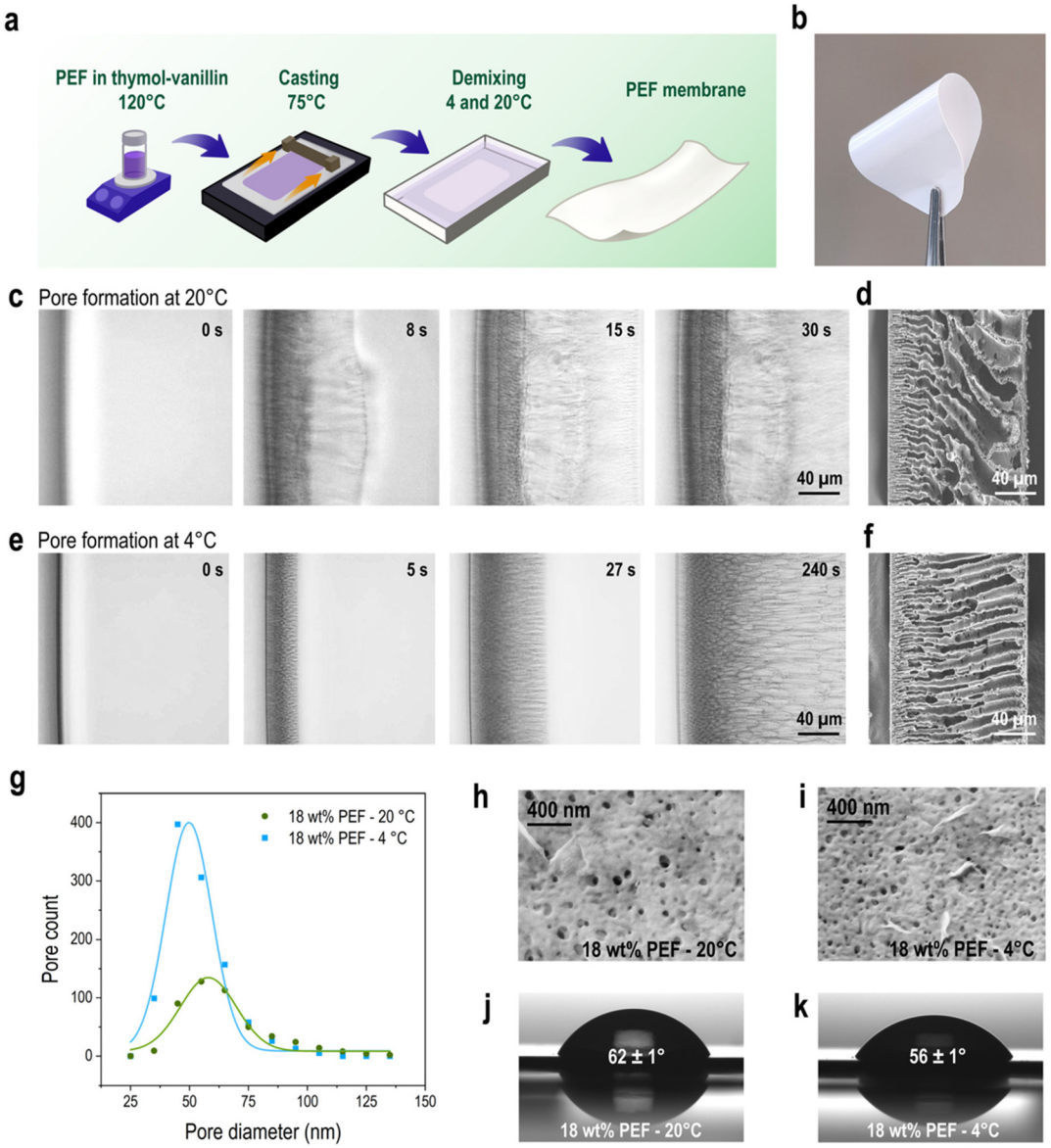

Fig. 2 PEF membrane fabrication and properties. (a) Schematic of the PEF membrane fabrication process. (b) Photograph of a flexible PEF membrane fabricated under optimized conditions (18 wt% PEF in thymol–vanillin precipitated in 4 °C ethanol). (c) PEF precipitation process from 18 wt% PEF in thymol–vanillin precipitated in ethanol at 20 °C and (d) resulting membrane morphology. (e) PEF precipitation process from 18 wt% PEF in thymol–vanillin precipitated in ethanol at 4 °C and (f) resulting membrane morphology. (g) Surface pore size distribution of PEF membranes obtained *via* surface micrographs analysis. (h and i) Surface micrograph of PEF membranes precipitated at 20 °C or 4 °C. (j and k) Water contact angle of PEF membranes precipitated at 20 °C or 4 °C.

driven by spinodal decomposition or nucleation and growth, depending on the thermodynamic conditions and kinetics of solvent exchange.[18] In addition, finger-like cavities are generated by the abrupt intrusion of the non-solvent into the dope solution, followed by fast demixing and solidification of the polymer-rich phase, which was the case for PEF membranes. The solution demixing was influenced by the polymer concentration and temperature. Higher temperature and lower polymer concentration led to faster solvent exchange and demixing. A clear demixing frontier was observed as the pores were formed. The fastest frontier moving rate was 16.38 µm s^{-1}, observed for 15 wt% PEF exposed to ethanol at 20 °C, while 21 wt% in ethanol at 4 °C resulted in the slowest rates (2.72 and 2.69 µm s^{-1}, respectively). The demixing rate directly influenced the membrane morphology, as observed by correlating the optical microscopy experiments with the scanning electron microscopy (SEM) images of the formed membranes (Fig. 2d and f, SI Fig. S16–S19). Large macrovoids were observed in the membranes coagulated at 20 °C, while at 4 °C they were significantly smaller.

The morphology and pore size distribution of the membranes varied with the preparation conditions, which influence

the solvent exchange rates (Fig. 2g–i and SI Fig. S19–S22-i). The analysis of SEM surface images with an AI-based model showed a mean surface pore size between 47 and 60 nm (Fig. 2g, SI Fig. S21). For all three polymer concentrations, a decrease in the coagulation bath temperature led to higher pore densities and smaller pore sizes, while an increase in polymer content resulted in lower pore densities. Not all pores imaged by SEM or atomic force microscopy (SI Fig. S19 and S20) are necessarily completely accessible for transport through the membrane. Therefore, the pore size was also measured *via* a gas–liquid displacement porometer. The effect of the coagulation bath temperature was more evident for membranes prepared from 15 wt% PEF solutions, with a mean pore size reduction from around 150 to 100 nm. Membranes prepared from 18 wt% PEF had smaller pores in the range of 50 to 150 nm (SI Fig. S22).

Varying the polymer concentration of the dope solution and the consequent pore sizes had a significant influence on the rejection profile of the membranes for molecules ranging from 10 to 300 kg mol^{-1} (Fig. 2g). Membranes obtained from 18 wt% at 4 °C had the highest poly(ethylene glycol) rejections with a molecular weight cut-off of 87 kg mol^{-1}, in the ultrafiltration range.

Varying the fabrication conditions also influenced the mechanical properties of the membranes, which were quantified in terms of Young's modulus, tensile strength, fracture strain, and toughness *via* strain *vs.* stress tests (SI Fig. S23). The membranes prepared from 18 wt% PEF solutions exhibited the highest values in all parameters, indicating superior mechanical stability. Therefore, the membranes prepared with 18 wt% PEF and coagulated at 4 °C (Fig. 2b), with a lower Young's modulus and low rigidity, were chosen for the subsequent studies.

A visual comparison of the hazards associated with the dope solution proposed in this work and other PEF dope solutions reported in the literature for membrane fabrication by electrospinning is depicted in Table 2. The comparison was made based on the chemical hazard pictograms retrieved from the safety data sheet and the grams of solvent components used in each case. The use of thymol and vanillin is associated with three hazard pictograms: irritant, corrosive, and environmental hazard, while the use of other combined fossil-based solvents also includes toxicity and health hazards. Adequate handling of the thymol–vanillin waste after membrane fabrication would prevent environmental damage. On the other hand, while the use of pure TFA displays only two hazard pictograms, it is highly volatile, moderately toxic, and persistent in the environment (Table 1). Overall, the utilization of thymol and vanillin is a safer alternative compared to the reported fossil-based solvents.

Table 2 Chemical hazards associated with solvents used for PEF dope solution preparation

Dope solution composition	Hazard pictograms (! = 1 g solvent / g PEF)	Ref.
18 wt% PEF		This work
65 wt% Thymol 17 wt% vanillin 20 wt% PEF		42 and 43
80 wt% TFA 12 wt% PEF		42
28 wt% TFA 60 wt% DE 12 wt% PEF		42
24 wt% TFA 64 wt% DM 12 wt% PEF		44
88 wt% HFIP 15 wt% PEF		45
71 wt% TFA 14 wt% HFIP		

TFA: trifluoroacetic acid, DE: 1,2 dichloroethane, DM: dichloromethane, and HFIP: hexafluoro-2-propanol.

Performance – juice clarification

The PEF membrane fabrication approach developed in this work employs non-toxic solvents, thereby aligning with sustainable and safe processing practices. Furthermore, the resulting optimized membranes had pore sizes and filtration performance (Fig. 2g and 3 and SI Fig. S21 and S22) in the ultrafiltration range and pronounced hydrophilicity, further confirmed by a water contact angle of 56 ± 1° (Fig. 2j and k, SI Fig. S24), making them well-suited for applications in the food and beverage processing industry. In particular, ultrafiltration membranes are increasingly deployed in fruit juice clarification, a crucial step for turbidity reduction and shelf lifetime extension of juice products.[73,74] The performance of PEF membranes for this application was therefore assessed using both dead-end and cross-flow filtration configurations.

Dead-end filtration with PEF membranes reduced the turbidity of all tested juices by more than 98% (Fig. 3c, SI Fig. S25). For pomegranate juice, the juice turbidity decreased by 98.7% with a final steady-state flux of around 10 L m^{-2} h^{-1} (SI Fig. S26), while the clarification of orange and apple juices resulted in a turbidity reduction of 99.8% with lower fluxes (Fig. 3b). Remarkably, the soluble solids expressed in °Brix and pH were largely preserved after clarification (SI Table S2), which is a positive indication of the presence of small molecules with nutritional value in the permeate. A gradual flux decline over time was observed, primarily due to surface fouling, which could potentially be mitigated by membrane backwashing (SI Fig. S27). Overall, the performance of the PEF

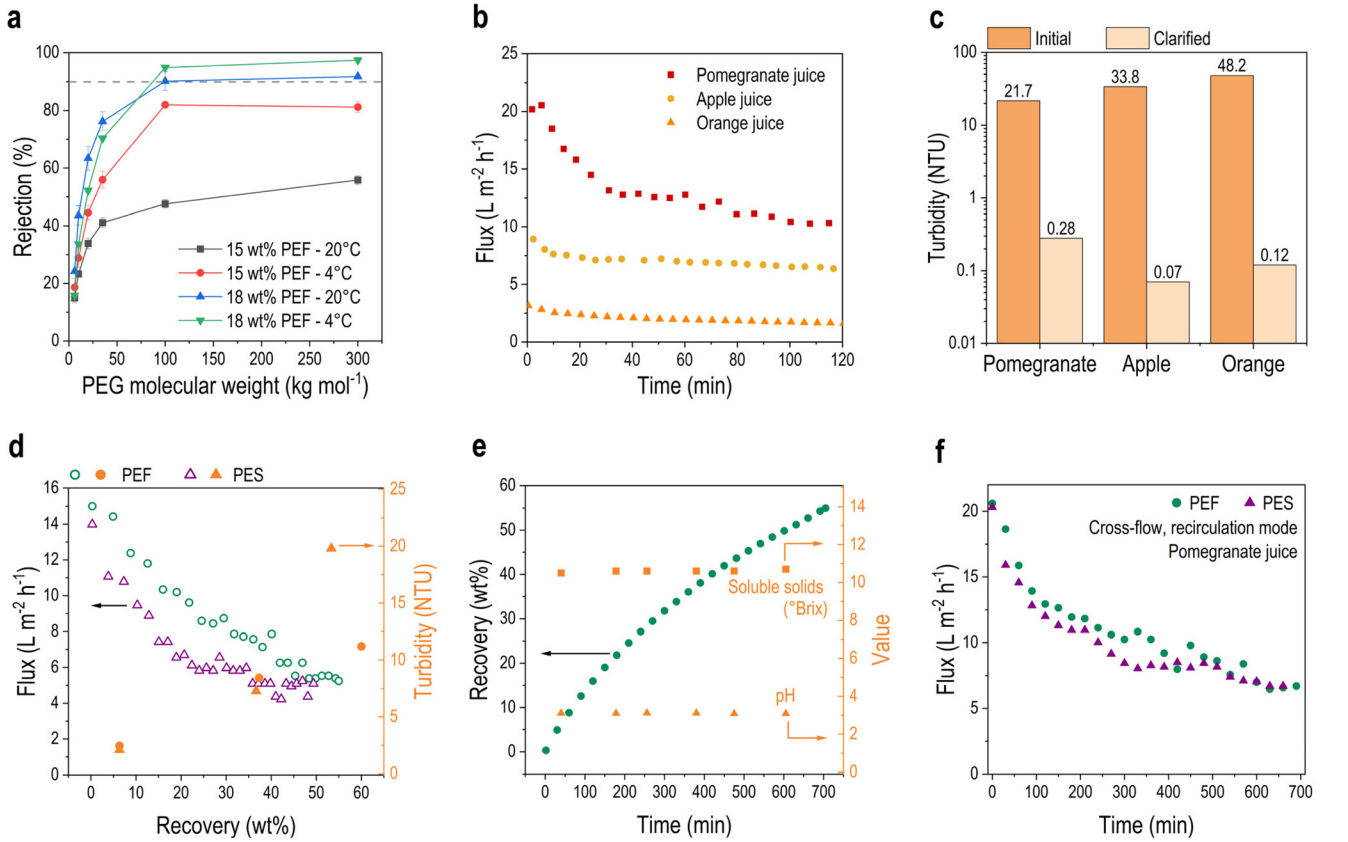

Fig. 3 Experimental filtration performance of bio-based PEF membranes. (a) Poly(ethylene glycol) rejection profiles of PEF membranes. (b) Juice flux during clarification with optimized PEF membranes (from 18 wt% PEF in thymol–vanillin precipitated at 4 °C) in the dead-end configuration. (c) Turbidity of the pomegranate, apple, and orange juices before and after clarification with PEF membranes in the dead-end configuration. (d) Experimental permeate flux and turbidity as a function of recovery rate during the cross-flow clarification of pomegranate juice using optimized PEF and commercial PES membranes. (e) Permeate recovery rate, soluble solids, and pH over time during cross-flow clarification of pomegranate juice using optimized PEF membrane. (f) Comparative experimental permeate fluxes of optimized PEF and commercial PES membranes measured under constant pomegranate juice feed in the cross-flow (recirculation/closed-loop) mode.

membrane in the dead-end configuration is competitive with commercial PES and PSf ultrafiltration membranes under the same experimental conditions (SI Fig. S26–S29).

For a more realistic evaluation of the performance of the bio-based PEF membrane, cross-flow filtration tests were performed and benchmarked against a commercial PES membrane. The PEF membrane allowed for a permeate recovery of nearly 60% after 700 min of operation, with higher flux and lower final permeate turbidity compared to the marketed PES membrane (Fig. 3d). During filtration, the pH and soluble solids remained stable (Fig. 3e, SI Tables S4 and S5). In an additional test, a 700-minute filtration test was performed in the recirculation mode to evaluate the long-term flux stability of the membrane with a constant pomegranate juice feed. The PEF membrane exhibited a flux decline from 20 to around 7 L m^{-2} h^{-1}, showing a comparable behavior to the commercial PES membrane (Fig. 3f).

Overall, these results indicate that the PEF membrane is a good candidate for natural juice clarification. Notably, all filtration experiments were performed at a very low applied pressure (0.2 bar), which represents a significant advantage in terms of energy consumption compared to conventional clarification methods such as centrifugation and thermal treatment.

Life cycle assessment

We evaluated the environmental profile of PEF membrane production employing an attributional LCA method with a cradle-to-gate perspective (Fig. 4a). The goal of the LCA study was to assess the environmental impact associated with the PEF membrane preparation protocol developed in this work, identifying the hotspots within the process and comparing it against the impacts of producing PET-based membranes prepared with TFA as the solvent. The PET membrane production process by NIPS was modelled following laboratory-scale conditions previously reported to obtain a molecular weight cut-off in the ultrafiltration range comparable to that obtained for the optimized PEF membrane.[16] Three PET types were assessed: pristine fossil-based, pristine partially bio-based (20% biogenic and 80% fossil C), and recycled PET.

In line with our objective of producing bio-based membranes, the feedstocks for polymer and solvent production

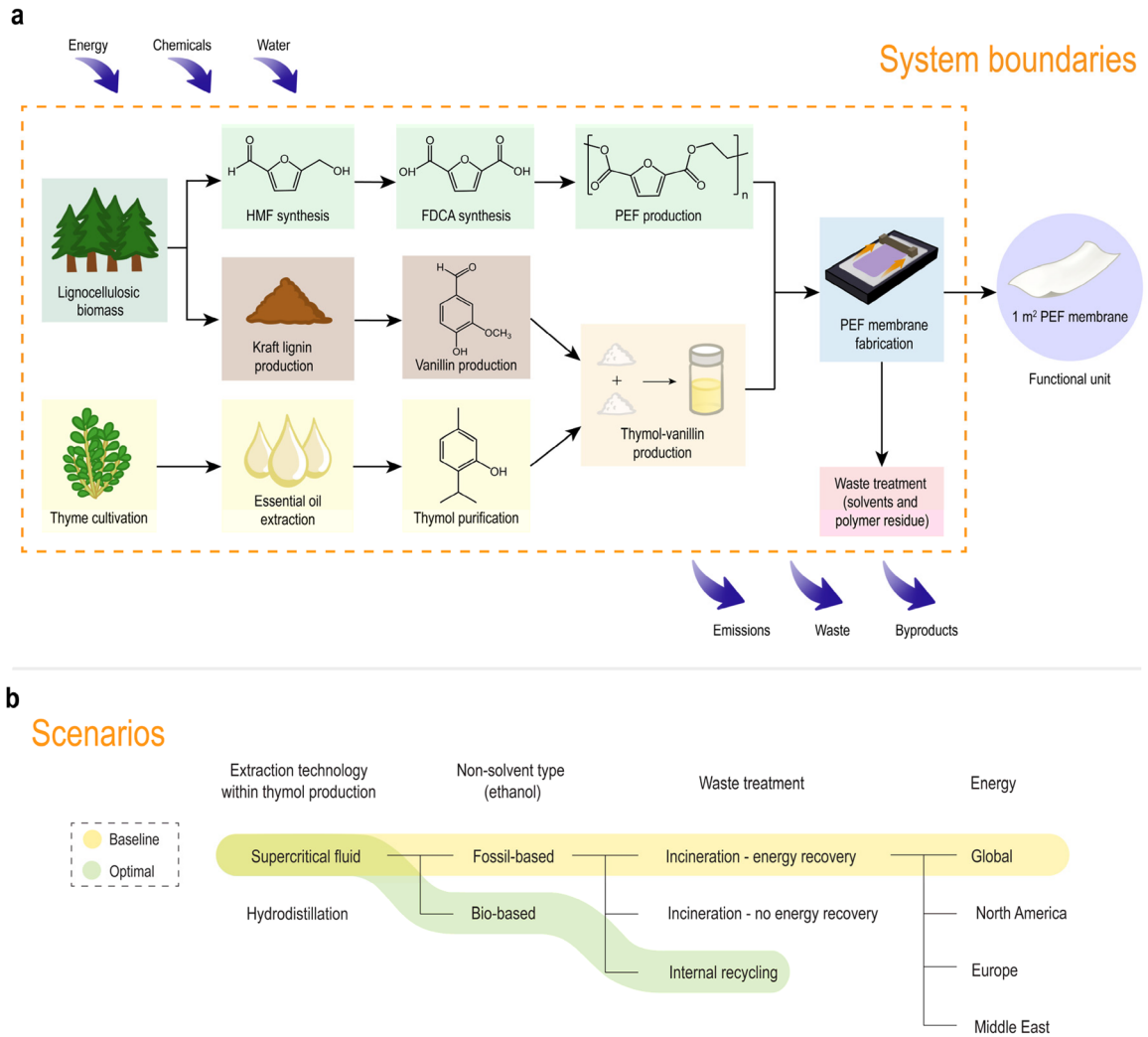

Fig. 4 Considerations in the cradle-to-gate LCA of PEF membrane production. (a) System boundaries for PEF membrane production with 1 m^2 as the functional unit. (b) Scenarios investigated.

were modeled as obtained from renewable sources: PEF and vanillin from lignocellulosic biomass obtained from forestry waste, and thymol from cultivated thyme plants (*Thyme vulgaris*). Different scenarios were explored to understand the effect of thymol production technologies, ethanol type, waste treatment, and energy geography scope (Fig. 4b, SI Tables S6 and S7). The Life Cycle Inventory is detailed in the SI (SI Fig. S30, SI Tables S9–S26), with data obtained from several sources.[16,37,75–82]

Given the significant mass contribution of thymol to the PEF-based dope solution, an initial comparison was made between hydrodistillation (HD) and supercritical fluid extraction (SFE) within the thymol production process. Our LCA analysis revealed that utilization of SFE for the extraction of thyme essential oil for the production of 1 kg of thymol led to lower environmental impacts on 18 out of the 19 categories (SI Fig. S31, Table S27). Similarly, the environmental impacts of the entire membrane production process with one or another method within the thymol production process were lower for SFE than for HD (SI Fig. S32, SI Table S28). These results can be related to the higher extraction yield and shorter processing times of SFE, as reported by several authors.[76,83,84] After this initial assessment, supercritical fluid extraction was adopted for the baseline scenario. The rest of the parameters were selected based on the standard practices in a laboratory setup: fossil-based ethanol as the non-solvent, incineration of the hazardous waste with energy recovery, and average global energy composition.

The production of 1 m^2 of PEF membrane in the baseline scenario resulted in Global Warming Potentials (GWPs) of 51.7 and 44.3 kg CO_2 eq. excluding and including biogenic carbon, respectively; a fossil depletion of 19.6 kg oil eq.; and land use of 33.38 annual crop eq. yr (SI Table S29). The membrane fabrication process was divided into subprocesses (SI Table S8), and the contribution of each one was quantified. Under these conditions, non-solvent production had the highest contribution in most of the categories (Fig. 5a). This result can be correlated with its high mass contribution compared to the

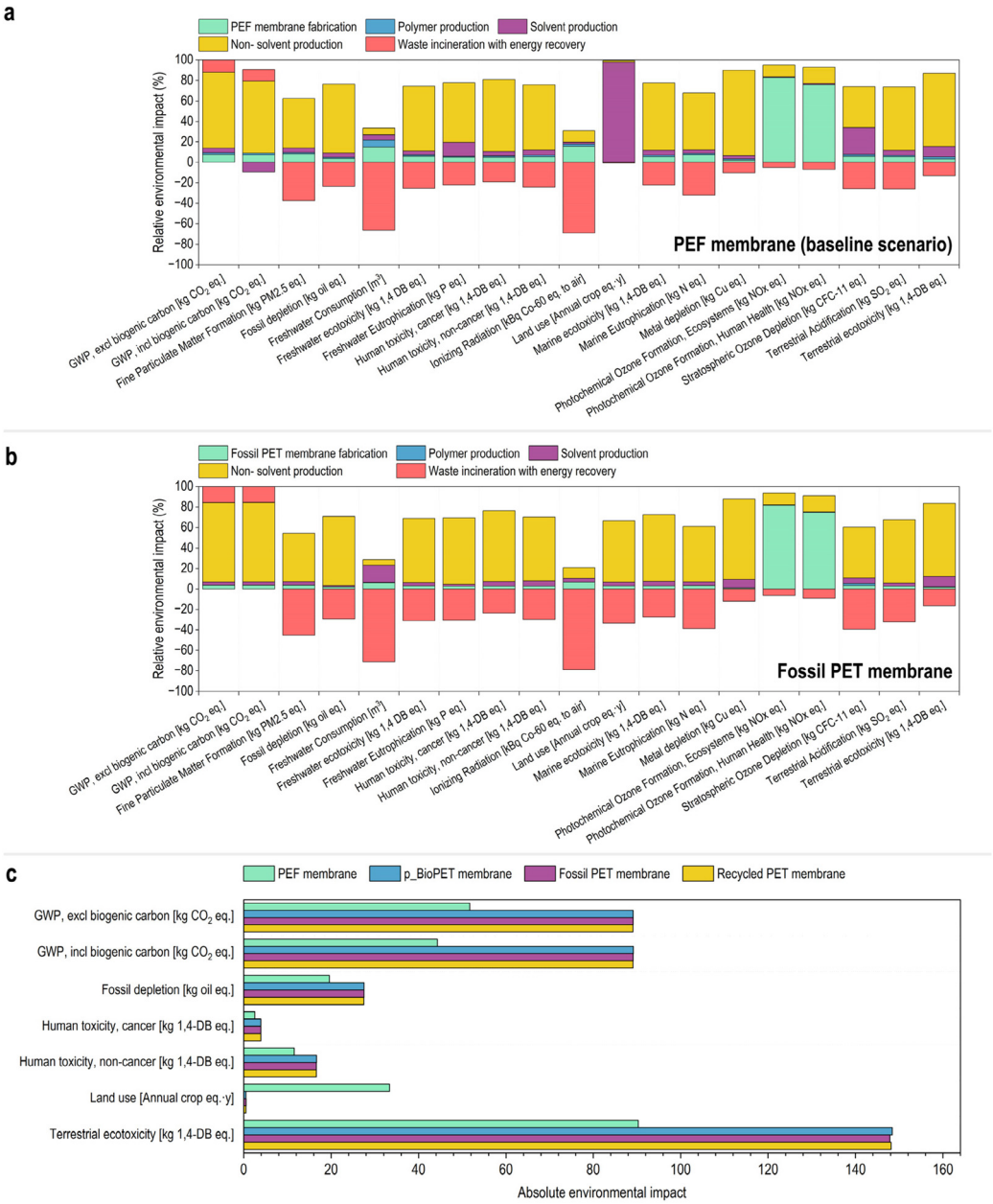

Fig. 5 Environmental impact of PEF and PET membrane production. (a) Subprocesses contribution for PEF membrane production in the baseline scenario. (b) Subprocess contribution for fossil PET membrane production (other parameters as the baseline scenario). (c) Comparison of the environmental impacts of PEF and different types of PET membrane production. The functional unit is 1 m^2 of membrane produced.

rest of the materials and the energy intensity of its production, given its fossil-based origin. In the GWP category, it accounted for 74% contribution, followed by waste treatment, PEF membrane production, solvent production, and polymer production. The solvent production had the highest impact on land use, which can be explained by the low thymol yield from thyme and the area required for its cultivation. Waste incineration with energy recovery compensated for some environmental impacts, such as fine particulate matter formation, freshwater consumption, and ionizing radiation due to the avoided additional electricity production given the energy-credit scheme utilized in our model.

Compared to PET membrane fabrication with trifluoroacetic acid as the solvent and the same assumptions for the ethanol type and waste treatment approach, the overall environmental impact of the PEF membrane was lower in most categories except for land use, freshwater consumption, ionizing radiation, and particulate matter formation (Fig. 5c, SI Fig. S33). The GWPs of the PEF membrane were 42% and 50% lower, excluding and including biogenic carbon, respect-

ively. Similar to PEF membranes, most of the environmental impact of PET membrane production was associated with non-solvent (also ethanol) production (Fig. 5b, SI Table S30). Regarding the contribution of individual subprocesses, the GWP of polymer production was lower for the PET membrane (0.1 against 0.95 kg CO_2 eq.), while the GWP of solvent production (TFA) was higher than the combined production of thymol and vanillin (2.74 against 2.31 kg CO_2 eq.). These differences arise from the material types and the fabrication conditions.

The PET type did not have a significant effect on the membrane environmental impact, given the small contribution of the polymer production subprocess, even though the impact per kg of polymer is the highest for fossil PET, followed by p_BioPET, and the lowest impact for recycled PET (Fig. S34 and Table S31).

Replacing fossil-based ethanol with a bio-based one (bioethanol) derived from fermentation processes had a significant effect on the environmental impacts of PEF membrane fabrication (Fig. S35). The GWP excluding biogenic carbon, including biogenic carbon, and fossil depletion decreased by 36%, 259% and 99%, respectively. However, other categories increased, such as freshwater ecotoxicity, freshwater consumption, land use, and terrestrial ecotoxicity. Nevertheless, in line with the motivation of this study to produce membranes from renewable feedstocks, this condition is still preferable relative to the conventional fossil-based route, and thus, was selected as part of the environmentally optimal scenario.

Given the large amount of solvent waste resulting from the membrane coagulation bath, two more waste treatment scenarios were compared with the baseline: (1) waste incineration without energy recovery; and (2) internal waste recycling coupled with energy recovery (Fig. S36). The lowest environmental impacts among the three scenarios were obtained with the internal recycling strategy (Fig. 6a). By this approach, the GWP, excluding biogenic carbon, was reduced by 54% compared to complete incineration with energy recovery and 69% compared to incineration without energy recovery. The reduction was even higher when including biogenic carbon (SI Fig. S37). This finding highlights the environmental relevance of minimizing solvent waste for more sustainable membrane manufacturing processes, as pointed out by several authors.[24,25,85,86]

Scenarios with different energy sources for the subprocesses of membrane fabrication and waste incineration with energy recovery were also modelled to investigate the variability of the impacts when fabricating the membrane in different geographical regions, namely North America, Europe, or the Middle East, which use different distributions of energy sources (SI Fig. S38 and S39, SI Table S33). If no step of energy recovery is considered, the lowest global warming potential is observed for Europe, followed by North America, and the highest for the Middle East. However, under an energy-credit approach, the net impact will be lower in the Middle East compared to Europe and North America regions because of the displacement of its more carbon-intensive energy grid (Fig. 6b, SI Fig. S40, SI Table S32).

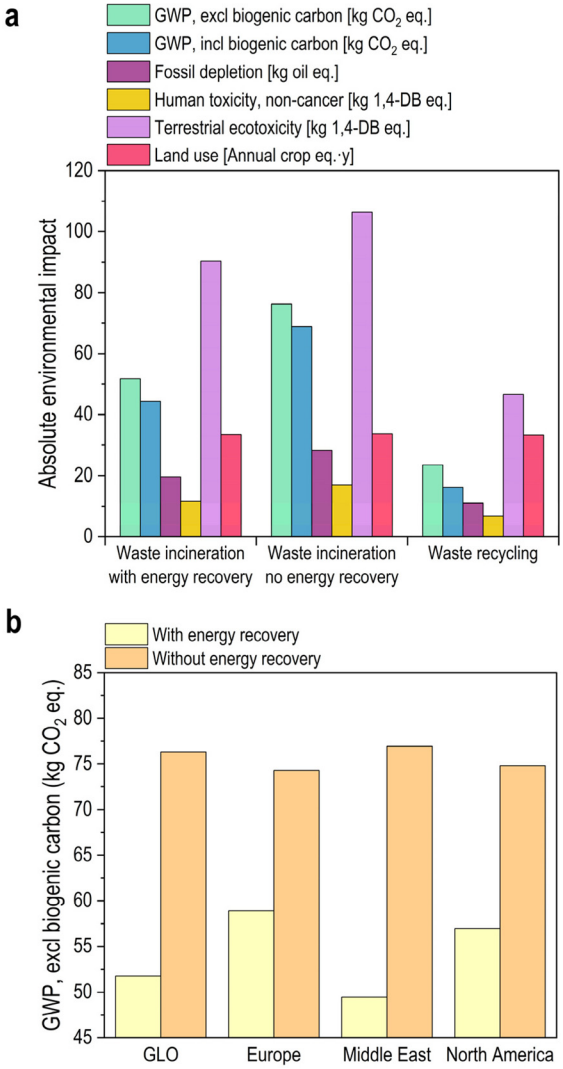

Fig. 6 Analysis of the effect of scenario conditions on the environmental impact of PEF membrane production. (a) Effect of waste treatment scenarios in climate change, fossil depletion, human toxicity (non-cancer), terrestrial ecotoxicity, and land use. (b) Effect of the geographical region for membrane fabrication and waste treatment on the Global Warming Potential (GWP) of the overall membrane production (baseline scenario). The functional unit is 1 m^2 of membrane produced.

Following previous studies, an environmentally optimal scenario for PEF membrane production conditions is proposed as follows: supercritical fluid extraction for thymol production, bio-EtOH as the non-solvent, and waste recycling. The environmental impact was dramatically lower in terms of GWP and fossil depletion compared to the baseline scenario, with GWP scores of 16.9 and −24.56 kg CO_2 eq. excluding and including biogenic carbon, respectively, and fossil depletion of 4.1 kg oil eq., strongly contrasting with the baseline scenario (51.7 kg CO_2 eq., 44.3 kg CO_2 eq., and 19.6 kg oil eq. for the same impacts). On the other hand, freshwater consumption, fresh-

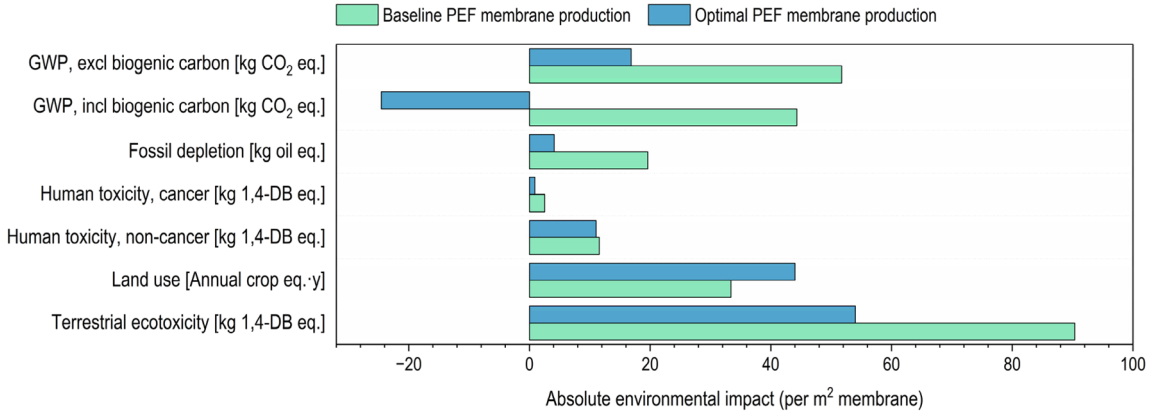

Fig. 7 Comparison between the baseline and optimal scenarios in terms of GWP, fossil depletion, human toxicity, land use, and terrestrial ecotoxicity. The functional unit is 1 m^2 of membrane produced.

water ecotoxicity, land use, marine eutrophication, and stratospheric ozone depletion exhibited higher values (Fig. 7, SI Table S34).

The results obtained here are, to the best of the authors' knowledge, the first LCA of PEF membranes, and thus, a direct comparison with the literature is not possible. However, other studies have assessed the environmental impact of substituting polymers or solvents for membrane fabrication by bio-sourced alternatives *via* LCA (SI Table S35). Most of these studies also found that this type of substitution can have positive effects in reducing the GWP of the membrane production process from 4 to 29% by either using bio-based polymers or replacing NMP with γ-butyrolactone, ethyl acetate, methyl lactate, DMSO, PolarClean, and ethylene carbonate.[54–57] It is noteworthy to witness that our bio-based strategy with optimized fabrication parameters reduces the GWP by 42% compared to a fossil-based counterpart, demonstrating the potential of PEF and thymol–vanillin as sustainable materials for membrane fabrication.

4. Conclusions

Given the need for the chemical industry to move away from fossil-based feedstocks and instead promote a bioeconomy, exploring the potential of PEF for high-performance applications can potentially improve the sustainability of several polymer-related industries, including membrane technology.[6,13,34]

In this work, we studied the suitability of naturally derived thymol and vanillin compounds to dissolve PEF, a biomass-derived polymer, and fabricate asymmetric porous membranes. We elucidated the interaction between the involved molecules by spectroscopic techniques, confirming that hydrogen bonding plays a key role in the formation of a thymol–vanillin deep eutectic mixture and the dissolution of PEF in both components. Under these conditions, vanillin exhibited keto–enol tautomerism, a phenomenon derived from hydrogen and electronic interactions among the involved molecules, resulting in varied colour profiles for the vanillin-based solutions. The membranes with the best performance were cast with 18 wt% PEF solutions in thymol–vanillin and coagulated in ethanol at 4 °C. The optimized PEF membranes were competitive in fruit juice clarification, with a flux of around 10 L m^{-2} h^{-1} even at a low pressure (0.2 bar), allowing for a turbidity reduction of around 99%, comparable to those of commercially available poly(ether sulfone) and polysulfone ultrafiltration membranes. While the application in the food sector was demonstrated, considering their inherent high chemical resistance, the PEF membranes developed in this work could be used in more challenging environments, such as in the chemical industry, for the filtration of solutions or particle dispersions (*e.g.* polymer latexes, stabilized colloidal particles, and crystallized pharmaceutical intermediates) of organic solvents. Further optimization of the fabrication to reduce the pore size would extend the application to organic solvent nanofiltration.

A comparative cradle-to-gate LCA study showed environmental advantages compared to fossil-based PET membranes.

Re-strategizing the membrane fabrication protocol for large-scale semi-continuous production of flat-sheet and hollow fiber PEF membranes compatible with current membrane manufacturing equipment remains an open challenge. In terms of LCA, more extensive life cycle inventory data of emerging bio-based materials are needed to further understand and advance the sustainability profile of bio-based membrane production.

Author contributions

Malinalli Ramírez-Martínez: conceptualization, methodology, investigation, validation, data curation, formal analysis, and writing – original draft. Usman T. Syed: conceptualization, investigation, supervision, and writing – review and editing. Glenda Terán-Cuadrado: investigation and writing – review and editing. Anissa Nurdiawati: supervision and writing –

review and editing. Maria Di Vincenzo: investigation and writing – review and editing; Iuliana M. Andrei: investigation; Sami G. Al-Ghamdi: resources. Dimitrios N. Bikiaris: investigation and resources. Suzana P. Nunes: conceptualization, methodology, resources, funding acquisition, project administration, supervision, and writing – review and editing.

Conflicts of interest

There are no conflicts to declare.

Data availability

The data supporting this article have been included as part of the supplementary information (SI). Supplementary information is available. See DOI: https://doi.org/10.1039/d5gc05422b.

Acknowledgements

This work was sponsored by the King Abdullah University of Science and Technology (KAUST) (grant OFP 2023 Grant 5614 "Sustainable membrane fabrication for organic solvent nanofiltration"). The authors acknowledge Prof. Volker C. Vahrenkamp for his support in optical microscopy observations.

References

1 S. B. Borrelle, J. Ringma, K. L. Law, C. C. Monnahan, L. Lebreton, A. McGivern, E. Murphy, J. Jambeck, G. H. Leonard and M. A. Hilleary, *Science*, 2020, **369**, 1515–1518.
2 J. W. Cottom, E. Cook and C. A. Velis, *Nature*, 2024, **633**, 101–108.
3 K. Houssini, J. Li and Q. Tan, *Commun. Earth Environ.*, 2025, **6**, 257.
4 Y. Zhu, C. Romain and C. K. Williams, *Nature*, 2016, **540**, 354–362.
5 K. Daehn, R. Basuhi, J. Gregory, M. Berlinger, V. Somjit and E. A. Olivetti, *Nat. Rev. Mater.*, 2022, **7**, 275–294.
6 F. Vidal, E. R. van der Marel, R. W. Kerr, C. McElroy, N. Schroeder, C. Mitchell, G. Rosetto, T. T. Chen, R. M. Bailey and C. Hepburn, *Nature*, 2024, **626**, 45–57.
7 R. M. Cywar, N. A. Rorrer, C. B. Hoyt, G. T. Beckham and E. Y.-X. Chen, *Nat. Rev. Mater.*, 2022, **7**, 83–103.
8 C. Shi, E. C. Quinn, W. T. Diment and E. Y.-X. Chen, *Chem. Rev.*, 2024, **124**, 4393–4478.
9 S. Pandey, B. S. Rajput and S. H. Chikkali, *Green Chem.*, 2021, **23**, 4255–4295.
10 A. C. Renner, S. S. Thorat and M. P. Sibi, *RSC Sustainability*, 2024, **2**, 3669–3703.
11 A. H. Menon, S. Joseph, M. H. Shaikh and S. H. Chikkali, *Macromol. Chem. Phys.*, 2025, e00113.
12 *Bioplastics: Synthesis, Characterization, and Applications*, ed. K. P. Shadangi, P. K. Sarangi, Apple Academic Press, New York, 1st edn, 2025.
13 L. T. Hao, S. Ju, D. K. Hwang, D. S. Hwang, Y. S. Ok, S. Y. Hwang, H. J. Kim, H. Jeon, J. Park and D. X. Oh, *Nat. Rev. Bioeng.*, 2024, **2**, 289–304.
14 P. Stegmann, V. Daioglou, M. Londo, D. P. van Vuuren and M. Junginger, *Nature*, 2022, **612**, 272–276.
15 J. Kim, J. F. Kim, Z. Jiang and A. G. Livingston, *Nat. Sustainability*, 2025, **8**, 594–605.
16 B. A. Pulido, O. S. Habboub, S. L. Aristizabal, G. Szekely and S. P. Nunes, *ACS Appl. Polym. Mater.*, 2019, **1**, 2379–2387.
17 S. Chisca, V.-E. Musteata, W. Zhang, S. Vasylevskyi, G. Falca, E. Abou-Hamad, A.-H. Emwas, M. Altunkaya and S. P. Nunes, *Science*, 2022, **376**, 1105–1110.
18 S. P. Nunes and T. Inoue, *J. Membr. Sci.*, 1996, **111**, 93–103.
19 S. P. Nunes and K.-V. Peinemann, *Membrane technology in the chemical industry*, John Wiley & Sons, 2006.
20 K. V. Pochivalov, A. V. Basko, T. N. Lebedeva, A. N. Ilyasova, M. Y. Yurov, R. Y. Golovanov, V. V. Artemov, V. V. Volkov, A. A. Ezhov and A. V. Volkov, *Mater. Today Commun.*, 2021, **28**, 102558.
21 A. Figoli, T. Marino, S. Simone, E. Di Nicolò, X.-M. Li, T. He, S. Tornaghi and E. Drioli, *Green Chem.*, 2014, **16**, 4034–4059.
22 M. Ramírez-Martínez, S. Aristizabal, L. Upadhyaya, A.-H. Emwas, N. Hadjichristidis and S. P. Nunes, *ACS Appl. Polym. Mater.*, 2024, **6**, 13120–13131.
23 D. Matveev, V. Vasilevsky, V. Volkov, T. Plisko, A. Shustikov, A. Volkov and A. Bildyukevich, *J. Environ. Chem. Eng.*, 2022, **10**, 107061.
24 D. Zou, S. P. Nunes, I. F. Vankelecom, A. Figoli and Y. M. Lee, *Green Chem.*, 2021, **23**, 9815–9843.
25 G. Szekely, *RSC Sustainability*, 2024, **2**, 871–880.
26 Z. Terzopoulou and D. N. Bikiaris, *Mater. Lett.*, 2024, **362**, 136174.
27 P. Tomietto, F. Russo, F. Galiano, P. Loulergue, S. Salerno, L. Paugam, J.-L. Audic, L. De Bartolo and A. Figoli, *J. Membr. Sci.*, 2022, **643**, 120061.
28 A. Y. Gebreyohannes, S. L. Aristizabal, L. Silva, E. A. Qasem, S. Chisca, L. Upadhyaya, D. Althobaiti, J. A. P. Coutinho and S. P. Nunes, *Green Chem.*, 2023, **25**, 4769–4780.
29 T. A. Otitoju, C.-H. Kim, M. Ryu, J. Park, T.-K. Kim, Y. Yoo, H. Park, J.-H. Lee and Y. H. Cho, *J. Cleaner Prod.*, 2024, **467**, 142905.
30 S. Kim, H. N. Thi, J. Kang, J. Hwang, S. Kim, S. Park, J.-H. Lee, M. H. Abdellah, G. Szekely and J. S. Lee, *Chem. Eng. J.*, 2024, **494**, 153201.
31 S. T. R. Velasquez, Q. Hu, J. Kramm, V. C. Santin, C. Volker and F. R. Wurm, *Angew. Chem., Int. Ed.*, 2025, **64**, e202423406.
32 J. J. Bozell and G. R. Petersen, *Green Chem.*, 2010, **12**, 539–554.

33 K. Loos, R. Zhang, I. Pereira, B. Agostinho, H. Hu, D. Maniar, N. Sbirrazzuoli, A. J. Silvestre, N. Guigo and A. F. Sousa, *Front. Chem.*, 2020, **8**, 585.
34 J.-G. Rosenboom, R. Langer and G. Traverso, *Nat. Rev. Mater.*, 2022, **7**, 117–137.
35 X. Fei, J. Wang, J. Zhu, X. Wang and X. Liu, *ACS Sustainable Chem. Eng.*, 2020, **8**, 8471–8485.
36 M. G. Davidson, S. Elgie, S. Parsons and T. J. Young, *Green Chem.*, 2021, **23**, 3154–3171.
37 A. Muralidhara, E. De Jong, H. A. Visser, G.-J. M. Gruter, C. Len, J.-P. Bertrand and G. Marlair, *ACS Omega*, 2022, **7**, 9181–9195.
38 S. K. Burgess, J. E. Leisen, B. E. Kraftschik, C. R. Mubarak, R. M. Kriegel and W. J. Koros, *Macromolecules*, 2014, **47**, 1383–1391.
39 C. Xu, X. K. Shi, L. J. Cui, S. J. Gao and S. P. Wu, *Biofuels, Bioprod. Biorefin.*, 2025, **19**, 2542–2580.
40 J.-G. Rosenboom, D. K. Hohl, P. Fleckenstein, G. Storti and M. Morbidelli, *Nat. Commun.*, 2018, **9**, 2701.
41 E. Uc-Fernández, R. Sulub-Sulub, A. González-Díaz, W. Herrera-Kao, A. Ávila-Ortega, E. Cetina-Mancilla, M. J. Aguilar-Vega and M. O. González-Díaz, *ACS Sustainable Chem. Eng.*, 2024, **12**, 10152–10163.
42 M. Svyntkivska, T. Makowski, E. L. de Boer and E. Piorkowska, *Polym. Test.*, 2022, **113**, 107677.
43 Y.-H. Huang, Y. Chang, C.-J. Huang, J.-M. Lin, S.-H. Tung, G.-W. Jang and C.-L. Liu, *Polymer*, 2024, **312**, 127619.
44 M. Svyntkivska, T. Makowski, R. Pawlowska, D. Kregiel, E. L. de Boer and E. Piorkowska, *Colloids Surf., B*, 2024, **233**, 113609.
45 K. Juraij, A. Niroula, Y. Greish, P. K. S. Mural, A. Nazir and M. Z. Iqbal, *J. Membr. Sci.*, 2025, **717**, 123622.
46 Z. Xu, K. Sanchez-Rivera, C. Granger, P. Zhou, A. D. C. Munguia-Lopez, U. M. Ikegwu, S. Avraamidou, V. M. Zavala, R. C. Van Lehn and E. Bar-Ziv, *Nat. Chem. Eng.*, 2025, **2**, 407–423.
47 S. Spatari, *Nat. Protoc.*, 2025, 1–2.
48 R. van Zelm, T. Hennequin and M. A. Huijbregts, *Nat. Protoc.*, 2025, 1–12.
49 S. Hellweg and L. Milà i Canals, *Science*, 2014, **344**, 1109–1113.
50 A. A. Martins, N. S. Caetano and T. M. Mata, *Sustainable Membrane Technology for Water and Wastewater Treatment*, 2017, pp. 23–66.
51 E. Khaki, H. Abyar, M. Nowrouzi, H. Younesi, M. Abdollahi and M. G. Enderati, *Environ. Technol. Innovation*, 2021, **22**, 101507.
52 F. Guyomarc'h, F. Héquet, S. Le Féon, N. Leconte, F. Garnier-Lambrouin, J. Auberger, C. Malnoë, C. Pénicaud and G. Gésan-Guiziou, *J. Food Eng.*, 2024, **380**, 112147.
53 M. I. Aydin and I. Dincer, *Energy*, 2022, **245**, 123090.
54 P. Yadav, N. Ismail, M. Essalhi, M. Tysklind, D. Athanassiadis and N. Tavajohi, *J. Membr. Sci.*, 2021, **622**, 118987–118987.
55 A. Fionah, I. Oluk, L. Brady, D. M. Byrne and I. C. Escobar, *Membranes*, 2024, **14**, 153.
56 S. U. Hong, Y. Wang, L. S. Soh and W. F. Yong, *Green Chem.*, 2023, **25**, 4501–4512.
57 F. Prézélus, J.-C. Remigy, C. Guigui and L. Tiruta-Barna, *J. Cleaner Prod.*, 2022, **337**, 130476.
58 J. Stanley, Z. Terzopoulou, P. A. Klonos, A. Zamboulis, E. Xanthopoulou, S. Koltsakidis, D. Tzetzis, L. F. Zemljič, D. A. Lambropoulou and A. Kyritsis, *Polymers*, 2023, **15**, 2707.
59 G. Z. Papageorgiou, G. N. Nikolaidis, R. O. Ioannidis, K. Rinis, D. G. Papageorgiou, P. A. Klonos, D. S. Achilias, M. Kapnisti, Z. Terzopoulou and D. N. Bikiaris, *ACS Sustainable Chem. Eng.*, 2022, **10**, 7050–7064.
60 U. T. Syed, L. Upadhyaya, L. M. D. Loiola, A. H. Emwas, A. Volkov and S. P. Nunes, *Green Chem.*, 2024, **26**, 11576–11586.
61 E. Cheve-Kools, Y. H. Choi, C. Roullier, G. Ruprich-Robert, R. Grougnet, F. Chapeland-Leclerc and F. Hollmann, *Green Chem.*, 2025, **27**, 8360–8385.
62 S. Soltani, H. Sereshti and N. Nouri, *Talanta*, 2021, **225**, 121983.
63 S. Mondal, U. T. Syed, C. Gil, L. Hilliou, A. F. Duque, M. A. Reis and C. Brazinha, *Green Chem.*, 2023, **25**, 1137–1149.
64 Y. P. Didion, T. Tjalsma, M. Malankowska, Z. R. Su, M. Matos, M. Pinelo, J. Crespo and C. Brazinha, *Chem. Eng. J.*, 2025, **511**, 161741.
65 H. Yamashita and J. Abe, *J. Phys. Chem. A*, 2014, **118**, 1430–1438.
66 R. Pis-Diez, G. A. Echeverría, O. E. Piro, J. L. Jios and B. S. Parajón-Costa, *New J. Chem.*, 2016, **40**, 2730–2740.
67 R. Kannan and V. Veeraragavan, *J. Mol. Struct.*, 2021, **1227**, 129521.
68 P. D. Beer and P. A. Gale, *Angew. Chem., Int. Ed.*, 2001, **40**, 486–516.
69 J. N. Israelachvili, *Intermolecular and surface forces*, Academic press, 2011.
70 N. M. Laurendeau, *Statistical thermodynamics: fundamentals and applications*, Cambridge University Press, 2005.
71 T. Anokhina, I. Borisov, A. Yushkin, G. Vaganov, A. Didenko and A. Volkov, *Polymers*, 2020, **12**, 2785.
72 M. Ramírez-Martínez, S. L. Aristizábal, G. Szekely and S. P. Nunes, *Green Chem.*, 2023, **25**, 966–977.
73 R. Sarbatly, J. Sariau and D. Krishnaiah, *Food Eng. Rev.*, 2023, **15**, 420–437.
74 B. Veleirinho and J. Lopes-da-Silva, *Process Biochem.*, 2009, **44**, 353–356.
75 Á. C. Sánchez, O. T. Berglihn, E. Ottaviano, T. Rücker, T. Pettersen, B. Wittgens, A. Aliko, L. Gálvez and M. López, *Open Res. Eur.*, 2024, **4**, 5.
76 D. V. Bermejo, I. Angelov, G. Vicente, R. P. Stateva, M. R. García-Risco, G. Reglero, E. Ibañez and T. Fornari, *J. Sci. Food Agric.*, 2015, **95**, 2901–2907.
77 F. Piccinno, R. Hischier, S. Seeger and C. Som, *J. Cleaner Prod.*, 2016, **135**, 1085–1097.

78 C. Moretti, R. Hoefnagels, M. van Veen, B. Corona, S. Obydenkova, S. Russell, A. Jongerius, I. Vural-Gürsel and M. Junginger, *J. Cleaner Prod.*, 2022, **343**, 131063.
79 S. Bello, I. Salim, P. Méndez-Trelles, E. Rodil, G. Feijoo and M. T. Moreira, *Holzforschung*, 2018, **73**, 105–115.
80 Z. Limam, C. Azzaro-Pantel, N. Hajjaji, M. Romdhane and J. Bouajila, *Comput. Chem. Eng.*, 2025, **200**, 109140.
81 A. I. Gavrila, C. G. Chisega-Negrila, L. Maholea, M. L. Gavrila, O. C. Parvulescu and I. Popa, *Agronomy*, 2023, **13**, 2331.
82 E. De Falco, M. Pergola, A. Vece, C. Angiuoni and G. Celano, *Ital. J. Agron.*, 2020, **15**, 1505.
83 N. F. Morsy, *Ind. Crops Prod.*, 2020, **145**, 112072.
84 C. Grosso, A. C. Figueiredo, J. Burillo, A. M. Mainar, J. S. Urieta, J. G. Barroso, J. A. Coelho and A. M. Palavra, *J. Sep. Sci.*, 2010, **33**, 2211–2218.
85 W. Xie, T. Li, A. Tiraferri, E. Drioli, A. Figoli, J. C. Crittenden and B. Liu, *ACS Sustainable Chem. Eng.*, 2021, **9**, 50–75.
86 C. Y. Loh, A. D. Burrows and M. Xie, *ACS ES&T Eng.*, 2025, **5**, 1882–1906.